Coupled spin Hall effect of ferrite/feromagnetic bilayer films and detection of microwave electromagnetic fields

Dai-Nan Zhang(张岱南), You-Bin Zheng(郑又彬), Xin-Kai Xu(徐鑫锴), Yi-Xin Wang(王益欣), Qing-Hui Yang(杨清慧), Huai-Wu Zhang(张怀武)

Citation: Chin. Phys. B. 35, 107504 (2026). DOI: 10.1088/1674-1056/ae24e8 | CSTR: 32038.14.CPB.ae24e8
http://cpb.iphy.ac.cn; http://iopscience.iop.org/cpb

What follows is a list of articles you may be interested in

Mixed spin states for strain-robust ferromagnetism in $SrCoO_3$ thin films

Xiquan Zheng(郑希诠), Nicholas B. Brookes, Flora Yakhou-Harris, Yingjie Lyu(吕英杰), Jianbing Zhang(张建兵), Qian Xiao(肖铅), Xinyi Jiang(蒋心怡), Qingzheng Qiu(仇清正), Qizhi Li(李齐治), Shilong Zhang(张世龙), Xinqiang Cai(蔡新强), Pu Yu(于浦), Yi Lu(卢毅), Yingying Peng(彭莹莹)

Chin. Phys. B. 35, 107501 (2026). DOI: 10.1088/1674-1056/ae881c | CSTR: 32038.14.CPB.ae881c

Magnetic proximity-induced magnetoresistance in $Pt/Tm_3Fe_5O_{12}$ heterostructures

Zhengguo Liang(梁正国), Kunjie Dai(戴坤杰), Qiming Lv(吕崎鸣), Ao Wang(王傲), Jinfeng Zhang(章金凤), Lingfei Wang(王凌飞)

Chin. Phys. B. 35, 077512 (2026). DOI: 10.1088/1674-1056/ae5788 | CSTR: 32038.14.CPB.ae5788

Efficient magnon transport and magnon torque through the epitaxial antiferromagnetic insulator α-Fe_2O_3

Donglin Song(宋东霖), Fanyu Meng(孟凡毓), Mingyang Sun(孙铭扬), Hongrui Ni(倪泓睿), Jinhao Zou(邹锦豪), Zichen Yao(姚子忱), Zhenlong Guo(郭振龙), Yichi Zhang(张一驰), Liyan Zhang(张丽艳), Hongliang Bai(白洪亮), Wenping Zhou(周文平), Yi Wang(王译)

Chin. Phys. B. 35, 047505 (2026). DOI: 10.1088/1674-1056/ae48c1 | CSTR: 32038.14.CPB.ae48c1

Thickness dependence of the magnetic properties of barium ferrite films prepared by pulsed laser deposition

Chengbo Zhao(赵诚博), Bowei Han(韩博纬), Yuchen Zhao(赵宇辰), Yang Sun(孙洋), Lichen Wang(王利晨), Ruoshui Liu(刘若水), Yunzhong Chen(陈允忠), Dengjing Wang(王登京)

Chin. Phys. B. 35, 027504 (2026). DOI: 10.1088/1674-1056/adf6a5 | CSTR: 32038.14.CPB.adf6a5

Current-driven magnetic domain wall motion in heterostructure films

Rui Fu(付瑞), Jiwen Chen(陈集文), Zichang Huang(黄子畅), Jingyi Guan(管璟一), Zidong Wang(王子东), Yan Zhou(周艳)

Chin. Phys. B. 34, 127502 (2025). DOI: 10.1088/1674-1056/ade4ad | CSTR: 32038.14.CPB.ade4ad

---

Coupled spin Hall effect of ferrite/feromagnetic bilayer films and detection of microwave electromagnetic fields

Dai-Nan Zhang(张岱南)[1,2], You-Bin Zheng(郑又彬)[1], Xin-Kai Xu(徐鑫锴)[1], Yi-Xin Wang(王益欣)[1], Qing-Hui Yang(杨清慧)[1], and Huai-Wu Zhang(张怀武)[1,2,†]

[1] *School of Electronic Science and Engineering, University of Electronic Science and Technology of China, Chengdu* 610054, *China*
[2] *State Key Laboratory of Electronic Thin Film and Integrated Devices, University of Electronic Science and Technology of China, Chengdu* 610054, *China*

(Received 30 July 2025; revised manuscript received 25 November 2025; accepted manuscript online 27 November 2025)

Designing novel spin-wave heterojunction materials and regulating their magnetic properties are key technologies for realizing spin quantum detection of microwave electromagnetic fields. In this study, a spin-wave heterojunction microwave electromagnetic field sensing detection scheme has been proposed, which modifies the inverse spin Hall effect (ISHE) by manipulating the magnetic moment distribution, anisotropic crystal field and ferromagnetic resonance line width (ΔH) of ferrite/ferromagnetic bilayer films. Then, the nanocrystalline DyCoNbZr/$Bi_1Dy_2Fe_5O_{12}$ bilayer films and the spin-wave heterojunction [Pt/DyCoNbZr/$Bi_1Dy_2Fe_5O_{12}$] were fabricated, and the effects of damping-like torque, field-like torque, and the ferrite underlayer on the magnetization distribution of the spin-wave heterojunction were analyzed. The results show that the excited microwave electromagnetic field signal can be detected with high sensitivity by inverse spin Hall voltage ($V_{\rm ISHE}$) detection of the spin wave heterojunction, and the $V_{\rm ISHE}$ is directly related to the amplitude, frequency, and phase of the microwave electromagnetic field. The spin–orbit interaction between the $Bi_1Dy_2Fe_5O_{12}$ and DyCoNbZr films can enable the films with low saturation magnetization to undergo an ISHE at low microwave excitation power, which lays a technical foundation for detecting the microwave electromagnetic fields using the ISHE.

Keywords: magnetic thin films, ferrite thin films, spin-wave heterojunction, magnetic moment

PACS: 75.70.Ak, 75.50.Cc, 75.30.Et, 75.60.Ej

DOI: 10.1088/1674-1056/ae24e8 **CSTR:** 32038.14.CPB.ae24e8

1. Introduction

The international research on controlled growth of large-size spin wave wafer thin film materials remains a technical challenge. Currently, the realization of such materials primarily relies on epitaxial growth of garnet ferrite thin films, such as yttrium iron garnet (YIG), on single-crystal gadolinium gallium garnet (GGG) substrates.[1–3] The predominant fabrication techniques include pulsed laser deposition (PLD) and RF magnetron sputtering.[4–6] However, YIG thin films grown using these methods generally exhibit higher magnetic damping factors than those produced by liquid-phase epitaxy (LPE), and more importantly, large-area epitaxial growth beyond 3-inch (1 inch = 2.54 cm) wafer scale remains unattainable. Schmidt *et al*.[4] fabricated YIG thin films with a thickness of 65 nm by PLD on GGG single-crystal substrates, and enhanced the crystalline quality of YIG materials (from amorphous to epitaxial single-crystal films) by post-annealing under argon, with a damping factor of 1.61×10^{-4}. At the Massachusetts Institute of Technology, Ross *et al*.[5–14] employed PLD to grow YIG thin films with thicknesses in the hundred-nanometer range on three different substrates (GGG, SGGG, and NGG), enabling spin-wave transmission via integrated waveguide excitation. However, fabricating large-size GGG wafers is extremely difficult, with controlling defect densities below 6 defects/cm^2 being a major technological hurdle for the future. Consequently, polycrystalline ferrite/ferromagnetic composite bilayer thin films have emerged as a promising alternative for future spin-wave integrated devices.[15,16]

Sandweg *et al*. demonstrated that exchange magnons could be coupled via spin pumping effects (SPE) and ISHE,[17–22] which can be detected in spin heterojunctions such as NiFe/PtPd, ferrite/Pt, and ferrite/ferromagnet/alloy structures. Their findings confirmed that the wavelength integration capability of these systems reaches the sub-micron scale, enabling the realization of spin-wave heterojunction devices.[23–28] Wang *et al*. investigated spin pumping in magnetically ordered ferrite thin films, including polycrystalline NiZn ferrite and polycrystalline YIG ferrite, as well as metal layers (Cu, Ag, Ta, W, Pt, and Au) with varying spin–orbit coupling strengths.[12] Their study measured the spin Hall angles of these metals and the interfacial spin-mixing conductance, revealing efficient spin pumping injection from ferrites to antiferromagnetic insulators such as NiO through strong coupling effects.[29–36] The magnetic damping factor of polycrystalline ferrite film ranges from 10^{-2} to 10^{-4}, enabling spin-wave transmission distances of up to centimeter scale at room temperature.[37–44] This makes them one of the most promising materials for realizing spin-wave-based functional

†Corresponding author. E-mail: hw.zhang@163.com

© 2026 Chinese Physical Society and IOP Publishing Ltd. All rights, including for text and data mining, AI training, and similar technologies, are reserved.

devices.

In this paper, novel spin-wave materials and effects are systematically studied, aiming to establish a theoretical framework for the design of magnetic properties of ferrite/ferromagnetic bilayer films. The Dy-doped CoNbZr ferromagnetic alloy film was chosen because it not only has in-plane and out-of-plane magnetic moment distributions,[45–47] but also adds anisotropy and spin–orbit manipulation after rare earth Dy atom doping, and the ferrite $Bi_xDy_{3-x}Fe_5O_{12}$ (Bi:DyIG, $x = 0.1$–1.0) was chosen because it is also a garnet film with in-plane and out-of-plane magnetic moment distribution, which can increase spin–orbit torque. In addition, both DyCoNbZr and Bi:DyIG polycrystalline films have damping coefficients of more than 10^{-2} and have gyromagnetic properties in the GHz frequency region, so the two films were selected for bilayer coupling. The research focuses on the optimization of the magnetization distribution, anisotropic crystal field, and damping factor of the bilayer film. In addition, by using the spin–orbit interaction at the heterojunction interface, the inverse spin Hall effect excited by a low microwave field is explored, which lays a foundation for the spin wave heterojunction detection of microwave electromagnetic field.

2. Magnetic coupling effect between ferrite/ferromagnetic bilayer films

This study seeks to improve the sensitivity and accuracy of spin-wave heterojunction-based microwave detection devices. The coupling between the ferrite film and ferromagnetic film will produce spin–orbit torque excitation in its total magnetic moment progression, and the spin–orbit effect makes the magnetic moment distribution of the bilayer film in the three-dimensional (x-, y-, z-directions) change, which leads to changes in the amplitude, frequency, and corresponding resonance magnetic field point of its V_{ISHE} signal. The magnetic moment distribution model of the spin-wave heterojunction constructed by a ferrite/ferromagnetic bilayer film on a silicon substrate or ferrite substrate is shown in Fig. 1(a). Among them, the nano-thickness CoNbZr ferromagnetic alloy thin film doped with rare earth Dy atoms has spatially distributed magnetic moments (both in-plane and out-of-plane), and the spinning ferrite films $(BiDy)_3Fe_5O_{12}$ also have both in-plane and out-of-plane magnetic moments. It can be constructed with ferromagnetic and ferrite films to form a composite bilayer film. According to the model in Fig. 1(a), the total magnetic moment of the composite bilayer films undergoes progression under the combined effect of the external magnetic field, microwave field, intrinsic magnetic field, demagnetization field, and spin–orbit interaction field. It is described by the Landau–Lifshitz–Gilbert equation[48]

$$\frac{\mathrm{d}\boldsymbol{M}}{\mathrm{d}t} = -\gamma\mu_0(\boldsymbol{M}\times\boldsymbol{H}_{\mathrm{eff}}) + \alpha\left(\boldsymbol{M}\times\frac{\mathrm{d}\boldsymbol{M}}{\mathrm{d}t}\right) + \tau_{\mathrm{ext}}, \quad (1)$$

where μ_0 represents the unit magnetic moment, γ is the spin-to-magnetic ratio factor, α is the damping coefficient, and $\boldsymbol{H}_{\mathrm{eff}}$ is all the equivalent magnetic fields acting on it in the magnetic moment progression. Here, we define τ_{ext} as the excitation term of the total magnetic moment $\boldsymbol{M}$ (m_x, m_y, m_z) precession induced by the spin–orbit interaction in the bilayer film. This excitation term is obtained through the curl (cross product) of the total magnetic moment $\boldsymbol{M}$, the spin torque $\boldsymbol{\sigma}$, the magnetic moment $\boldsymbol{m}_1$ (m_{1x}, m_{1y}, m_{1z}) and $\boldsymbol{m}_2$ (m_{2x}, m_{2y}, m_{2z}) of the ferromagnetic and ferrite thin film[48]

$$\tau_{\mathrm{ext}} = \tau_{\mathrm{SOT}} = \gamma\mu_0 H_{\mathrm{DL}}(\boldsymbol{M}\times\boldsymbol{\sigma}\times\boldsymbol{m}_2) + \gamma\mu_0 H_{\mathrm{FL}}(\boldsymbol{M}\times\boldsymbol{\sigma}). \quad (2)$$

The first term represents a damping-like torque, with H_{DL} denoting the damping-like field. The second term corresponds to a field-like torque, where H_{FL} represents the field-like strength. When the magnetic moment precession approaches a steady state under the excitation of the external field, internal field, and spin–orbit field, meaning that it no longer varies with time, equations (3) are set to zero.

$$\begin{aligned}\frac{\mathrm{d}\boldsymbol{M}}{\mathrm{d}t} &= -\gamma\mu_0 + \alpha\left(\boldsymbol{M}\times\frac{\mathrm{d}\boldsymbol{M}}{\mathrm{d}t}\right) + \gamma\mu_0 H_{\mathrm{DL}}(\boldsymbol{M}\times\boldsymbol{\sigma}\times\boldsymbol{m}_2)\\ &\quad + \gamma\mu_0 H_{\mathrm{FL}}(\boldsymbol{M}\times\boldsymbol{\sigma}), \quad (3)\\ \frac{\mathrm{d}m_x}{\mathrm{d}t} &= \left[-\gamma\mu_0(m_y H^z_{\mathrm{eff}} - m_z H^y_{\mathrm{eff}}) + \alpha\left(m_y\frac{\mathrm{d}m_z}{\mathrm{d}t} - m_z\frac{\mathrm{d}m_y}{\mathrm{d}t}\right)\right.\\ &\quad + \gamma\mu_0 H_{\mathrm{DL}}(m_x m_{2x}\sigma\cos\varphi_1 - \sigma_x m_x m_{2x}\cos\varphi_2)\\ &\quad \left.+ (m_y\sigma_z - m_z\sigma_y)\right], \quad (4)\\ \frac{\mathrm{d}m_y}{\mathrm{d}t} &= \left[-\gamma\mu_0(m_x H^z_{\mathrm{eff}} - m_z H^x_{\mathrm{eff}}) + \alpha\left(m_x\frac{\mathrm{d}m_z}{\mathrm{d}t} - m_z\frac{\mathrm{d}m_x}{\mathrm{d}t}\right)\right.\\ &\quad + \gamma\mu_0 H_{\mathrm{DL}}(m_y m_{2y}\sigma\cos\varphi_1 - \sigma_y m_y m_{2y}\cos\varphi_2)\\ &\quad \left.+ \gamma\mu_0 H_{\mathrm{DL}}(m_x\sigma_z - m_z\sigma_x)\right], \quad (5)\\ \frac{\mathrm{d}m_z}{\mathrm{d}t} &= \left[-\gamma\mu_0(m_x H^y_{\mathrm{eff}} - m_y H^x_{\mathrm{eff}}) + \alpha\left(m_x\frac{\mathrm{d}m_y}{\mathrm{d}t} - m_y\frac{\mathrm{d}m_x}{\mathrm{d}t}\right)\right.\\ &\quad + \gamma\mu_0 H_{\mathrm{DL}}(m_z m_{2z}\sigma\cos\varphi_1 - \sigma_z m_z m_{2z}\cos\varphi_2)\\ &\quad \left.+ \gamma\mu_0 H_{\mathrm{FL}}(m_x\sigma_y - m_y\sigma_x)\right]. \quad (6)\end{aligned}$$

The relationship between the magnetic moment component ratios m_x/m_y, m_z/m_y, and m_z/m_x exerted by the microwave field of the composite bilayer film can be obtained. The term $\cos\varphi_1$ represents the angle between the total $\boldsymbol{M}$ and the $\boldsymbol{m}_2$ of the ferrite layer, while $\cos\varphi_2$ denotes the angle between the total $\boldsymbol{M}$ and the spin torque $\boldsymbol{\sigma}$, as shown in Fig. 1(a).

Based on the LLG equation, the anisotropic field and magnetic moment (m_x, m_y, m_z) of the double-layer thin film were numerically simulated with the change of the magnetic moment m_{2x} (in-plane magnetic moment of ferrite film), H_{DL} and H_{FL} fields. The ferromagnetic resonance linewidth (ΔH) is a function of the damping coefficient, saturation magnetization, anisotropic field, and driving magnetic field. After measuring the damping coefficient α of the double-layer

film prepared by different processes, the variation of the ΔH with frequency and anisotropic field coefficient was calculated based on the Matlab software, as shown in Fig. 1(b). We performed simulation calculations to analyze the relative distribution variations of the total magnetic moment components m_x, m_y, and m_z in the composite bilayer film. Additionally, we conducted theoretical calculations to evaluate their influence on the ΔH. As shown in Figs. 1(c) and 1(d), the m_{2x}, m_{2y}, and m_{2z} correspond to the magnetization components of the ferrite thin film, H_{DL} represents the damping-like field, and H_{FL} denotes the field-like strength.

From Fig. 1(b), it can be seen that significant ΔH occurs only when the ratio m_x/m_y is within the range of 0.8 to 1.4, indicating that the planar anisotropy field coefficient $k = m_x/m_y$ must be between 0.8 and 1.4 to induce noticeable ferromagnetic resonance absorption and generate spin-wave effects. As the frequency (f) increases from 0.2 GHz to 20 GHz, the ΔH increases from 235 Oe to 255 Oe. In Fig. 1(c), it can be observed that the out-of-plane magnetic moment m_z of the composite bilayer film shows a parabolic trend with the increase of the magnetic moment m_{2x} of the ferrite underlying film and the field-like strength H_{FL}. As m_{2x} increases from 500 Gs to 2000 Gs and H_{FL} increases from 50 Oe to 200 Oe, the ratio m_z/m_y rises from 0.15 to 0.45. The ratio m_z/m_y increases linearly with either m_{2x} or H_{FL}, but the growth trend is steeper for the m_{2x}, indicating that the out-of-plane magnetization of the composite bilayer film is enhanced with increasing ferrite bottom layer magnetization m_{2x}. For Fig. 1(d), when m_{2x} increases from 100 Gs to 1000 Gs, m_x/m_y sharply rises from 0.1 to 1.0 and then gradually increases to 1.2. This suggests that the in-plane easy-axis magnetization of the composite bilayer film is not significantly affected by the variation of the damping-like field H_{DL}, but it increases rapidly with the enhancement of the ferrite layer m_{2x}. These calculation results show that the magnetic moment distribution (m_x/m_y and m_z/m_y) of the bilayer film can be changed by the spin–orbit coupling field H_{FL} and in-plane magnetic moment m_{2x} of the ferrite thin film, which in turn regulates the ferromagnetic resonance linewidth ΔH, damping absorption α and the strength of the ISHE of the spin-wave heterojunction.

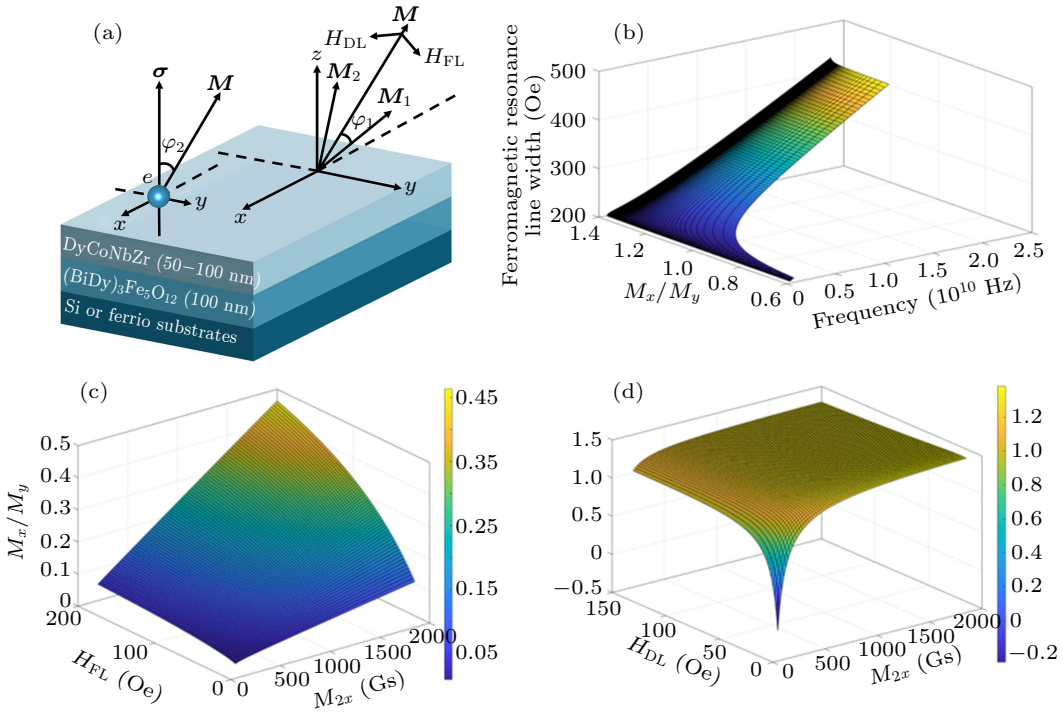

Fig. 1. (a) Magnetic moment distribution of the bilayer film and the heterojunction structure, (b) variation of the ΔH with m_x/m_y and microwave frequency f, (c) and (d) variations of m_x, m_y, and m_z distributions with m_{2x}, H_{DL}, and H_{FL}. The unit 1 Oe = 79.5775 A·m^{-1}, 1 Gs = 10^{-4} T.

3. Composite bilayer film samples preparation and performance test analysis

First, ferrite thin films ($Bi_1Dy_2Fe_5O_{12}$) were deposited on ferrite ceramic substrates or Si substrates using RF magnetron sputtering, and then the 100-nm-thick ferrite films were annealed and crystallized by rapid cycle annealing at a temperature of 650 °C–800 °C; the thin film grain size was controlled at about 80 nm–120 nm. The Dy-doped CoNbZr amorphous thin films were magnetron sputtered on the surface of the ferrite thin films, and then the Dy-CoNbZr thin films were crystallized through rapid cycle annealing at temperatures between 350 °C and 600 °C, forming nanocrystalline grains with well-defined surface morphology, resulting in a composite bilayer thin-film structure. The sputtering conditions were as follows: the target material was 4-inch $Bi_xDy_{3-x}Fe_5O_{12}$ ($x = 1.0$–1.4)

ferrite and CoNbZr alloy target (Co:85.5 at.%, Nb:8.9 at.%, Zr:5.6 at.%, and Dy was the metal patch); the backing vacuum was $\leq 1.0 \times 10^{-4}$ Pa, the sputtering gas pressure was 5×10^{-1} Pa, the sputtering power was 100 W, the sputtering rate was 50 nm/min, and the substrate temperature was ≤ 60 °C. The microstructure of the thin films was analyzed using a Bede D10 multifunctional x-ray diffractometer (XRD). The hysteresis loops were measured using an alternating gradient magnetometer (AGM). The surface morphology, grain size, and domain structures of the films were investigated using a SEIKO SPA-300HV scanning probe microscope (SPM) in atomic force microscopy (AFM) mode.

The Dy-doped CoNbZr films with thicknesses of 30 nm–150 nm were subjected to nano crystallization under different annealing temperatures while keeping the heating rate ($\alpha = 50$ °C/s), cycle number ($N = 6$ cycles), and dwell time ($t_a = 1$ min) constant. The annealing temperatures were set to 475 °C, 500 °C, 525 °C, and 550 °C. Figure 2(a) presents the XRD patterns of the Dy-CoNbZr samples annealed at different temperatures with identical cycle numbers and dwell times. The as-deposited films grown at room temperature exhibit an amorphous structure. At 475 °C, crystalline grains begin to precipitate, showing a preferential α-Co (0002) orientation. As the annealing temperature increases, the diffraction peaks become sharp, and the full width at half maximum decreases, indicating grain growth. According to the Scherrer equation, the estimated grain size of the DyCoNbZr film ranges from 30 nm to 80 nm (not more than 100 nm). The resistivity of the thin films is directly related to the grain size, and remains around 0.43×10^{-5} Ω·m. The magnetic moment components m_x, m_y, and m_z test results are shown in Figs. 2(b) and 2(c). Here, m_x, m_y, and m_z are obtained by applying magnetic fields in three different directions (x, y, z directions) and using an oscillating sample magnetometer (VSM) to test the hysteresis loops and remanent magnetization in each direction. The m_x of the bilayer film increases from a small 789 Gs to a maximum 841 Gs, and then decreases with the increase of annealing temperature from 350 °C to 600 °C, m_y decreases from 55.6 Gs (350 °C) to 20.6 Gs (450 °C) and then increases to 41 Gs (550 °C) as the annealing temperature increases from 350 °C to 550 °C, the m_z decreases from 28 Gs (350 °C) to 12 Gs (517 °C), and then increases to 41 Gs (576 °C). In-plane and out-of-plane magnetization VSM test results confirm that the three-dimensional (3D) magnetic moment distribution of the bilayer film is consistent with the magnetic moment distribution calculations in the second part. The hysteresis loop measurements under an external magnetic field applied along the easy magnetization axis and after annealing at different temperatures reveal that the coercivity of the bilayer film is temperature-dependent, a sudden change in the hysteresis loops occurs during the grain formation, indicating that larger grains significantly influence the film's saturation magnetization, coercivity, and magneto crystalline anisotropy field. The purpose of doping rare-earth Dy atoms is to enhance the anisotropy field H_k of the CoNbZrDy/Bi:DyIG films, because the uniaxial anisotropy field of rare-earth Dy is the largest, thereby enabling the control of the ferromagnetic resonance linewidth ΔH.

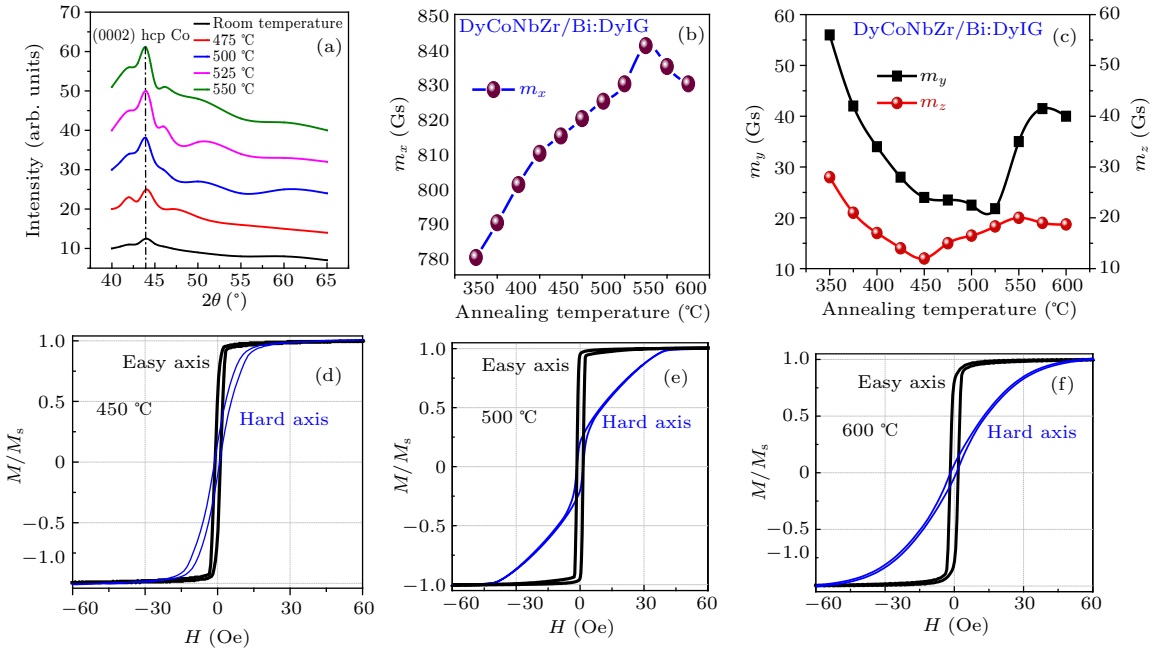

Fig. 2. (a) XRD patterns curves of the Dy-CoNbZr film under different annealing temperatures; (b) the m_x measurements of the bilayer film at different crystallization temperatures, (c) the magnetic moment component of the bilayer film m_y and m_z varies with the annealing temperature, (d) isotropic field H_k in-plane measurement along the hard and easy magnetization axes 450 °C, (e) 500 °C, and (f) 600 °C. Here m_x, m_y, m_z, and M_s are x, y, and z component magnetic moments of the total magnetic moment $\boldsymbol{M}$, and saturation magnetic moments, respectively.

Figures 2(d)–2(f) present the measurement results of the anisotropy field H_k at different temperatures. As the annealing temperature increases, the slope of the hysteresis loop along the hard magnetization axis becomes steeper, indicating that the in-plane anisotropy field H_k increases accordingly. The variation of H_k with annealing temperature suggests that rapid thermal processing significantly enhances the in-plane anisotropy field of the as-deposited DyCoNbZr/Bi:DyIG films, increasing its value from 15 Oe to 45 Oe. It is proved that the anisotropic crystal field can be changed by manipulating the grain size. The maximum value of the easy-axis m_x is about 810 Gs, the hard axis m_y is about 56 Gs, and the vertical m_z is about 28 Gs, all of which vary with the annealing crystallization temperature. For annealing temperatures above 450 °C, nanocrystals begin to form, and localized Co_5Dy intermetallic compounds emerge within Dy-surrounding clusters. The incorporation of a small amount of rare-earth Dy into the nanocrystalline CoNbZr thin film enhances the single-ion anisotropy constant, thereby increasing the in-plane uniaxial anisotropy of the thin film.

To further prove that there is a magnetic moment in the vertical direction of the bilayer film, Fig. 3 presents the magnetic domain structures of CoNbZrDy/Bi:DyIG bilayer films subjected to post-annealing treatment at different temperatures. As shown in Fig. 3(a), after annealing at 350 °C, stripe domains appear on the film surface, indicating the presence of perpendicular magnetic anisotropy (PMA), while the bending of these domains suggests residual stress within the film. At 400 °C (Fig. 3(b)), the stripe domains become weaker and more linear, implying that annealing effectively reduces residual stress, leading to a decrease in PMA and a concomitant increase in in-plane magnetic anisotropy (IMA). The annealing temperature of 450 °C (Fig. 3(c)) represents a critical threshold, where PMA completely vanishes and residual stress is almost eliminated, resulting in well-defined IMA. Further increasing the annealing temperature to 500 °C–600 °C (Figs. 3(d)–3(f)) leads to a complete absence of stripe domains, confirming a dominant in-plane magnetization state. Although the films undergo nano crystallization at these elevated temperatures, the grain size remains too small to generate sufficient stress to induce perpendicular stripe domains. These findings demonstrate that rapid thermal annealing effectively modulates the magnetic anisotropy of DyCoNbZr/Bi:DyIG films, thereby optimizing their magnetic properties.

Here, the anisotropy field H_k originates from single-particle anisotropy, the incorporation of rare-earth Dy into films, and magnetic coupling between garnet ferrite/ferromagnetic bilayer films, leading to an increase in both H_k and coercivity, with a further enhancement as the Dy concentration increases. The $(CoNbZr)_{1-x}Dy_x$/Bi:DyIG films with a low Dy concentration (3%) exhibit both soft magnetic and gyromagnetic properties, with a slight decrease in saturation magnetization (M_s = 840 Gs) and a coercivity field of approximately 3 Oe.

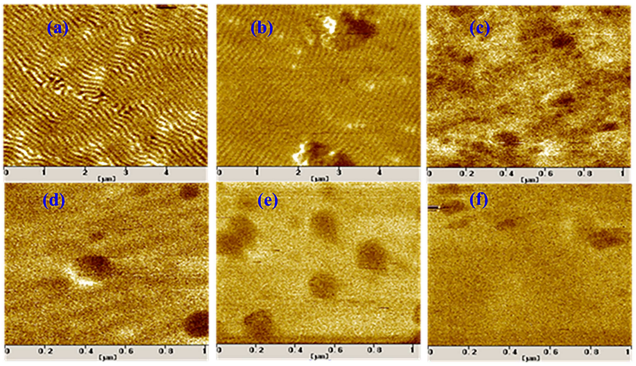

Fig. 3. Surface magnetic domains of DyCoNbZr/Bi:DyIG thin films after rapid annealing at different temperatures: (a) 350 °C, (b) 400 °C, (c) 450 °C, (d) 500 °C, (e) 550 °C, (f) 600 °C.

4. Inverse spin Hall effect in CoNbZrDy/Bi:DyIG composite bilayer films

In order to study a spin wave heterojunction as an electromagnetic field sensor to detect space microwave fields, a 10-nm heavy metal Pt layer was deposited on the surface of the DyCoNbZr/Bi:DyIG bilayer film to constitute a spin-wave heterostructure. Subsequently, the Pt layer was patterned into a Hall device using photolithography and etching techniques, as illustrated in Fig. 4(a). The microwave signal received by the antenna is amplified and then introduced into the coplanar waveguide (CPW), with the spin wave heterojunction positioned atop the CPW to facilitate microwave excitation. The microwave electromagnetic field induced precession of the magnetic moments in the DyCoNbZr/Bi:DyIG bilayer film, generating a spin current that subsequently produced a V_{ISHE} at both ends of the Pt layer. The ferromagnetic resonance linewidth (ΔH) of the DyCoNbZr/Bi:DyIG bilayer films was measured across different microwave frequency bands, as shown in Fig. 4(b). The frequency-swept ΔH spectra of the bilayer films reveal that for frequencies from 10 GHz to 18 GHz, the amplitude of the ΔH signal decreases with increasing frequency, while the resonance field shifts to higher values, indicating a broadening of the ΔH with frequency. The ΔH is 252.0 Oe at 10 GHz, the corresponding resonant field is 800 Oe, the maximum anisotropy field is H_k =45 Oe, the saturation magnetization is $4\pi M_s = 10569.5$ Gs, and the damping coefficient α is less than 1×10^{-2}, consistent with the calculation results of Section 2. Figure 4(c) presents the V_{ISHE} measured under an 8-GHz microwave excitation at varying microwave power and resonance magnetic field.

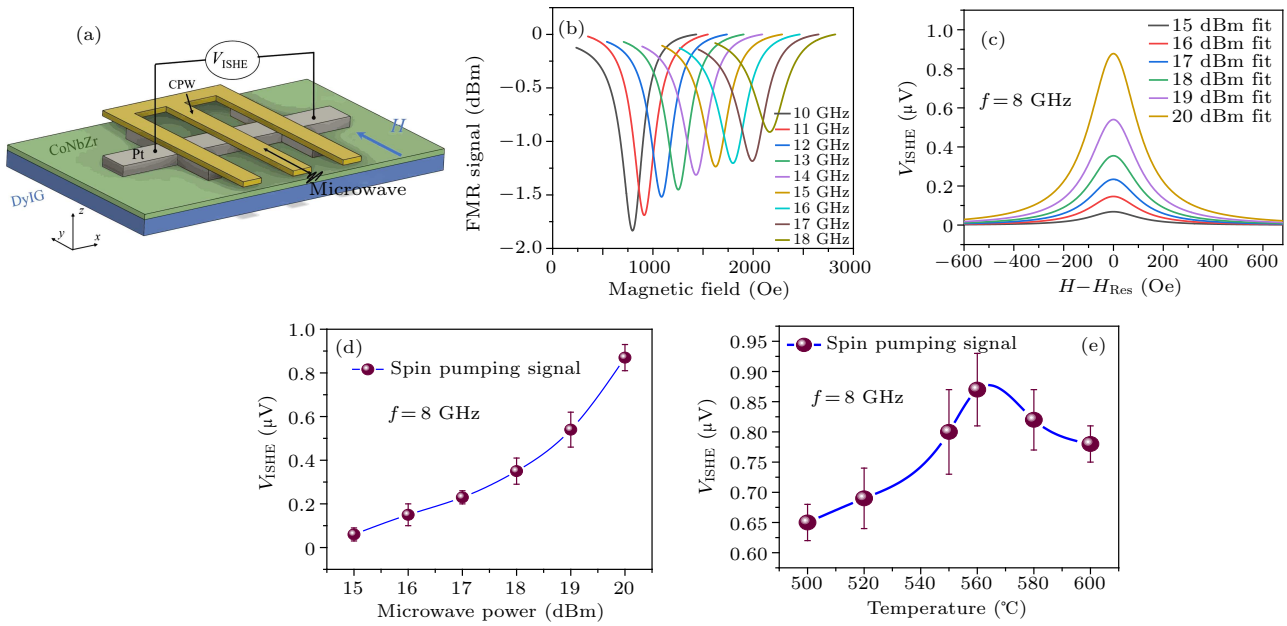

Fig. 4. (a) The ISHE of the [Pt/DyCoNbZr/Bi:DyIG] heterojunction, (b) 10 GHz–18 GHz FMR signal sweep test, (c) the V_{ISHE} signal varies with the resonant magnetic field, (d) variation of the V_{ISHE} with microwave power, (e) variation of V_{ISHE} with annealing temperature.

As shown in Figs. 4(c)–4(e), the spin wave heterojunction [Pt/DyCoNbZr/Bi:DyIG] generates a significant V_{ISHE} when the amplified microwave power exceeds 15 dBm. This shows that the weak microwave signal received by the antenna can be detected as long as it is amplified to 15 dBm. The V_{ISHE} increases as the excitation power increases. It can be seen that as long as the V_{ISHE} value and the magnetic field point of the V_{ISHE} curves resonance are measured, we can detect the amplitude, frequency, and phase of the excitation microwave field. The microwave power required to induce the V_{ISHE} is closely related to the magnetic moment distributions m_x, m_y, m_z, and resonance frequency points of the heterojunction. At a measurement frequency of 8 GHz and a sample annealing temperature of more than 500 °C in Fig. 4(d), in-plane $4\pi M_s$ (m_x, m_y) is a critical factor influencing V_{ISHE}, as a decrease in $4\pi M_s$ necessitates a higher microwave excitation power. Figure 4(e) presents the measured V_{ISHE} values for [Pt/DyCoNbZr/Bi:DyIG] heterojunctions fabricated under different annealing temperatures. The results indicate that within the annealing temperature range of 500 °C to 600 °C, the V_{ISHE} signal varies between 0.65 μV and 0.87 μV, with the maximum V_{ISHE} voltage of 0.87 μV achieved at an optimal annealing temperature of 560 °C. This enhancement is attributed to the ability of rapid annealing to modulate the grain size, thereby altering the saturation magnetization (m_x, m_y, and m_z distributions), anisotropy field (H_k), and damping coefficient (α) of the magnetic thin film. Therefore, optimizing the spin Hall effect can be achieved through precise control of the magnetic properties of the bilayer film. Under the certain size and structure of the heterojunction, the main factors affecting VISH are the saturation magnetization, spin–orbit torque equivalent magnetic field, and damping coefficient of the bilayer film. The ferromagnetic resonance linewidth is related to the damping coefficient, anisotropic crystal field, and saturation magnetization. Therefore, in order of importance of the impact are saturation magnetization $4\pi M_s$, the H_{FL}, and ferromagnetic resonance linewidth ΔH.

To further validate the influence of vertical magnetic moment distributions m_z and spin–orbit interaction (H_{FL}) on the V_{ISHE} signal, we investigated spin–orbit coupling between amorphous Dy-CoNbZr films and $Bi_xDy_{3-x}Fe_5O_{12}$ ($x = 0.8$–1.2) ferrite films. The aim is to design a spin-wave heterojunction sensor with higher sensitivity for electromagnetic field detection. The purpose of low-temperature annealing of thin films is to keep the film in an amorphous state and possess vertical magnetic domains, as shown in Fig. 4, allowing us to determine the threshold microwave excitation power required to induce spin waves in amorphous or partially amorphous thin films. Additionally, the spin–orbit coupling (H_{FL}) of the low-temperature bilayer film is used to adjust the vertical magnetization component m_z and reduce the in-plane saturation magnetization $4\pi M_s$, so that the spin–orbit coupling is enhanced to reduce the required microwave excitation power, enabling an investigation of the ISHE driven by spin torque H_{FL} in bilayer films. The V_{ISHE} of the low-temperature [Pt/DyCoNbZr/Bi:DyIG] heterojunction was characterized, as shown in Fig. 5.

From Fig. 5, it can be observed that V_{ISHE} signals were detected in all three samples, those without annealing, three cycles annealing at 380 °C for 30 mins, and annealed for a single cycle of 20 mins under a microwave excitation power about 16 dBm–26 dBm. The results show that the spin-wave heterojunction constructed by the magnetic coupling of the amorphous Dy-CoNbZr film with distribution of vertical magnetic

moment and the garnet ferrite Bi:DyIG polycrystalline film with a thickness of 100 nm still has an obvious spin Hall effect, which can be used as a sensor for microwave electromagnetic field detection. Moreover, V_{ISHE} increased with prolonged annealing time, with values of 0.4 μV for the non-annealed sample, 0.65 μV for the 20-minute annealed sample, and 1.0 μV for the 30-minute annealed sample, as shown in Fig. 5(c). The V_{ISHE} of all three samples exhibited a nonlinear increase with rising microwave excitation power, shown in Fig. 5(d). Within the power range of 16 dBm to 26 dBm, the optimal variation of V_{ISHE} was between 0.5 μV and 2.8 μV. These results further confirm that spin–orbit coupling (H_{FL}) between the bilayer composite films significantly influences the spin Hall effect, and this is consistent with the theoretical calculation of the H_{FL} field effects in Section 2. Even with reduced saturation magnetization in the ferromagnetic thin film, an obvious spin Hall effect can still be achieved by leveraging the H_{FL} within the bilayer system. From the simulation calculations in Section 2, it can be seen that H_{FL} mainly affects the distribution of m_z/m_y, which helps to enhance the inverse spin Hall voltage signal. This finding highlights the potential for controlling the crystallographic phase, magnetic properties, damping coefficient, and anisotropy field of the thin films to fine-tune the performance of spin-wave heterojunction devices. Furthermore, the spin–orbit coupling torque field at the interface of the ferrite/ferrimagnet bilayer can assist in magnetization switching of low-saturation magnetic moment thin films, thereby reducing the required microwave excitation power and improving the sensitivity of spin-wave heterojunction sensors to detect microwave electromagnetic fields.

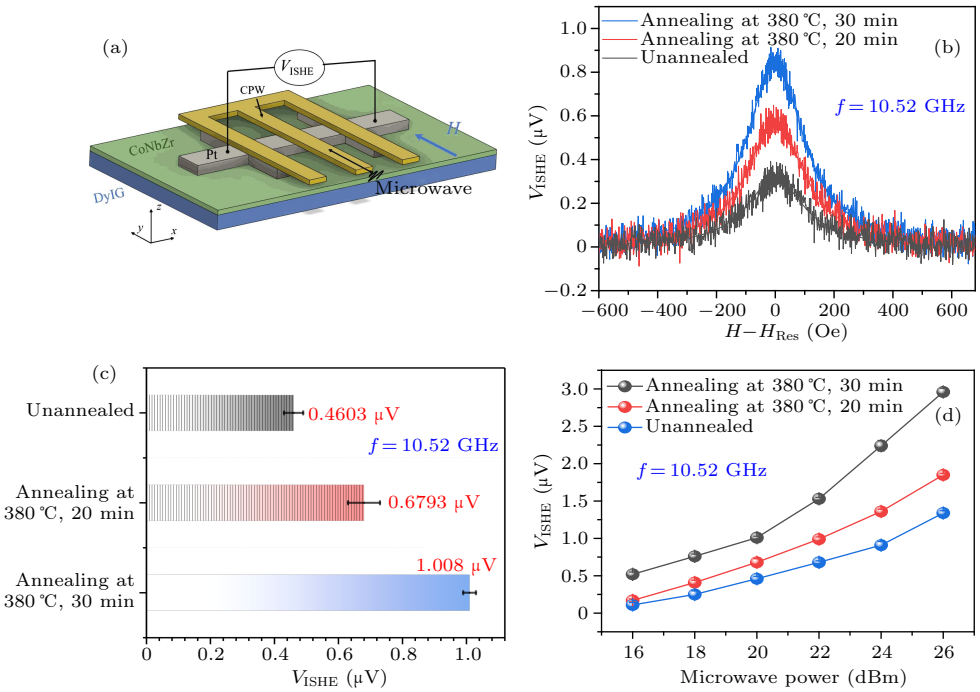

Fig. 5. (a) The ISHE test for low-temperature [Pt/Dy-CoNbZr/Bi:DyIG] heterojunction, (b) the V_{ISHE} test curves of 380 °C, 0-min, 20-min, and 30-min annealings at microwave power of 20 dBm, (c) comparison of the V_{ISHE} values of 0-min, 20-min, and 30-min samples at microwave power of 20 dBm, (d) the variation of the V_{ISHE} strength variation with microwave power.

5. Conclusion

In order to develop a microwave electromagnetic field-detecting spin-wave Hall device closer to practical use, this paper investigates the spin-wave heterojunction of ferrite/ferromagnetic composite bilayer thin films, and analyzes the effects of spin–orbit coupling between the composite bilayer on the film's magnetic moments, anisotropic fields, damping coefficients, and ferromagnetic resonance linewidths, and finds that nano granularized DyCoNbZr thin films, as well as the doping of rare earth Dy ions can change the magnetization $\boldsymbol{M}$ (m_x, m_y, m_z), anisotropic field H_k and ferromagnetic resonance linewidth of the composite bilayer films, the spin–orbit interaction between the [Bi:DyIG/DyCoNbZr] bilayer films can enable the films with low saturation magnetization in-plane to undergo an ISHE at low microwave excitation power, which provides a way for ferrite Bi:DyIG films and amorphous DyCoNbZr film with vertical magnetic domains to be applied in spin-wave heterojunction devices, and constructed [Pt/DyCoNbZr/Bi:DyIG] heterojunction can improve the sensitivity of microwave electromagnetic field sensing and detection. The control of the magnetic moment distribution, the anisotropic crystal field, and the ferromagnetic resonance linewidth, which increases the saturation magnetization, spin–orbital torque field and mixed conductivity real part of the heterojunction, therefore, the inverse spin Hall effect is enhanced. The magnitude of the V_{ISHE} can be regulated by the coupling-

induced magnetic energy change between the bilayer films, which lays a technical foundation for detecting the magnitude, frequency, and phase of microwave electromagnetic fields in space using the ISHE.

Acknowledgements

Project supported by the National Natural Science Foundation of China (Grant Nos. 52572154, 52272137, 62271106, and 52472146) and the National Key Research and Development Program of China (Grant No. 2022YFB3608300).

References

[1] Chumak A V, Vasyuchka V I, Serga A and Hillebrands B 2015 *Nat. Phys.* **11** 453
[2] Kajiwara Y, Harii K, Takahashi S, Ohe J, Uchida K, Mizuguchi M, Umezawa H, Kawai H, Ando K, Takanashi K, Maekawa S and Saitoh E 2010 *Nature* **464** 262
[3] Zhang Z, Jin L, Wen T, Liao Y, Tang X, Zhang H and Zhong Z 2020 *Scientia Sinica Informationis* **50** 67
[4] Hauser C, Eisenschmidt C, Richter T, Muller A, Deniz H and Schmidt G 2017 *J. Appl. Phys.* **122** 083908
[5] Yoshimoto T, Goto T, Shimada K, Iwamoto B, Nakamura Y, Uchida H, Ross C A and Inoue M 2018 *Adv. Electron. Mater.* **4** 1800106
[6] Sun Y, Song Y Y, Chang H, Kabatek M, Jantz M, Schneider W, Wu M, Schultheiss H and Hoffmann A 2012 *Appl. Phys. Lett.* **101** 152405
[7] Dubs C, Surzhenko O, Linke R, Danilewsky A, Brückner U and Dellith J 2017 *J. Phys. D: Appl. Phys.* **50** 204005
[8] Förster F, Gräfe J, Bailey J, Finizio S, Träger N, Groß F, Mayr S, Stoll H, Dubs C, Surzhenko O, Liebing N, Woltersdorf G, Raabe G J, Weigand M, Schütz G and Wintz S 2019 *Phys. Rev. B* **100** 214416
[9] Fu J, Hua M, Wen X, Xue M, Ding S, Wang M, Yu P, Liu S, Han J, Wang C, Du H, Yang Y and Yang J 2017 *Appl. Phys. Lett.* **110** 202403
[10] Sandweg C W, Kajiwara Y, Chumak A V, Serga A A, Vasyuchka V I, Jungfleisch M B, Saitoh E and Hillebrands B 2011 *Phys. Rev. Lett.* **106** 216601
[11] Kapelrud A and Brataas A 2013 *Phys. Rev. Lett.* **111** 097602
[12] Wang H L, Du C H, Pu Y, Adur R, Hammel P C and Yang F Y 2014 *Phys. Rev. Lett.* **112** 197201
[13] Wang H L, Du C H, Hammel P C and Yang F Y 2014 *Phys. Rev. Lett.* **113** 097202
[14] Rao Y, Zhang D, Zhang H, Jin L, Yang Q, Zhong Z, Hong L C and Ma B 2018 *J. Phys. D: Appl. Phys.* **51** 435001
[15] Jin L, Jia K, He Y, Wang G, Zhong Z and Zhang H 2019 *Appl. Surf. Sci.* **483** 947
[16] Liu M, Jin L, Zhang J, Yang Q, Zhang H, Gao P and Yu D 2018 *AIP Adv.* **8** 085117
[17] Bai H, Zhan X Z, Li G, Su J, Zhu Z Z, Zhang Y, Zhu T and Cai J W 2019 *Appl. Phys. Lett.* **115** 182401
[18] Chumak A V, Serga A A and Hillebrands B 2014 *Nat. Commun.* **5** 4700
[19] Wang Q, Pirro P and Verba R 2018 *Sci. Adv.* **4** 1701517
[20] Rumyantsev S, Balinskiy M, Kargar F, Khitun A and Balandin A A 2019 *Appl. Phys. Lett.* **114** 090601
[21] Cornelissen L J, Liu J and Wees B J 2018 *Phys. Rev. Lett.* **120** 097702
[22] Cramer J, Fuhrmann F, Ritzmann U, Gall V, Niizeki T, Ramos R, Qiu Z, Hou D, Kikkawa T, Sinova J, Nowak U, Saitoh E and Kläui M 2018 *Nat. Commun.* **9** 1089
[23] Collet M, Milly X, Allivy Kelly O D, Naletov V V, Bernard R, Bortolotti P, Youssef J B, Demidov V E, Demokritov S O, Prieto J L, Muñoz M, Cros V, Anane A, Loubens G D and Klein O 2016 *Nat. Commun.* **7** 10377
[24] Zanganeh S, Hutter G, Spitler R, Lenkov O, Mahmoudi M, Shaw A, Pajarinen J S, Nejadnik H, Goodman S and Moseley M 2016 *Nat. Nanotech.* **11** 986
[25] Qin H, Both G J, Hämäläinen S J, Yao L and Dijken S V 2018 *Nat. Commun.* **9** 5445
[26] Li Y, Polakovic T, Wang Y L, Xu J, Lendinez S, Zhang Z, Ding J, Saglam T H, Divan R, Xiao Z, Novosad V, Hoffmann A and Zhang W 2019 *Phys. Rev. Lett.* **123** 107701
[27] Han H, Zhang P, Hou J T, Siddiqui S A and Liu L 2019 *Science* **366** 1121
[28] Wang Y, Zhu D, Yang Y, Lee K, Mishra R, Go G, Oh S H, Kim D H, Cai K, Liu E, Pollard S D, Shi S, Lee J, Teo K L, Wu Y, Lee K J and Yang H 2019 *Science* **366** 1125
[29] Yan P, Wang X S and Wang X R 2011 *Phys. Rev. Lett.* **107** 177207
[30] Liu C, Chen J, Liu T, Heimbach F, Yu H, Xiao Y, Hu J, Liu M, Chang H, Tu S, Zhang Y, Gao P, Liao Z, Yu D, Xia K, Lei N, Zhao W and Wu M 2018 *Nat. Commun.* **9** 738
[31] Lin B, Wang S, Wang A, Li Y, Li R, Xia K, Yu D and Liao Z 2020 *Phys. Rev. Lett.* **124** 116802
[32] Sun Y, Abid A Y, Tan C, Ren C, Li M, Li N, Chen P, Li Y, Zhang J, Zhong X, Wang J, Liao M, Liu K, Bai X, Zhou Y, Yu D and Gao P 2019 *Sci. Adv.* **5** 4355
[33] Xiao J and Bauer G E W 2012 *Phys. Rev. Lett.* **108** 217204
[34] Yu W, Lan J and Xiao J 2020 *Phys. Rev. Appl.* **13** 024055
[35] Lan J, Yu W and Xiao J 2017 *Nat. Commun.* **8** 178
[36] Jin L, Wang Y, Lu G, Li J, He Y, Zhong Z and Zhang H 2019 *AIP Adv.* **9** 025301
[37] Rao Y, Zhang D, Jin L, Zhong Z, Yang Q, Li M, Li J, Yang Y, Wang G, Gan G and Zhang H 2019 *J. Magn. Magn. Mater.* **490** 165442
[38] Rao Y, Zhang D, Jin L, Zhong Z, Yang Q, Li M, Li J, Yang Y, Wang G, Gan G and Zhang H 2020 *J. Magn. Magn. Mater.* **497** 165817
[39] Zhang Z, Liu S, Zhang D, Jin L, Liao Y and Zhong Z 2020 *J. Phys. D: Appl. Phys.* **53** 105002
[40] Liu S C, Jing LC, Yang Q H, Wang X R, Zhang D N and Zhang H W 2023 *ACS Electronic Materials* **5** 3410
[41] Ren Z, Liu S, Jin L, Wen T, Liao Y, Tang X, Zhang H and Zhong Z 2019 *Sci. Rep.* **9** 7093
[42] Wang L, Gao L, Jin L, Liao Y, Tang X, Zhang H and Zhong Z 2018 *AIP Adv.* **8** 055103
[43] Liu C, Wu S, Zhang J, Chen J, Ding J, Ma J, Zhang Y, Sun Y, Tu S, Wang H, Liu P, Li C, Jiang Y, Gao P, Yu D, Xiao J, Duine R, Wu M, Nan C W, Zhang J and Yu H 2019 *Nat. Nanotech.* **14** 691
[44] Wu H, Huang L, Fang C, Yang B S, Wan C H, Yu G Q, Feng J F, Wei H X and Han X F 2018 *Phys. Rev. Lett.* **120** 097205
[45] Zhou C, Yuan S K, Zhu D Y, Bai Y M, Wang T, Liu F F, Pan L L, Feng C F, Zhang B H, He D P and Wang S X 2024 *Chin. Phys. B* **33** 037506
[46] Fan Y Y, Wang J, Hu F X, Li B H, Geng A C, Yin Z, Zhang C, Zhou H B, Wang M Q, Yu Z B and Shen B G 2023 *Chin. Phys. B* **32** 087504
[47] Liu Q, Lu X Y, Fu C R, Chen J R, Zhang Z, Gong Y T, Wang X Y, Yan Y, Gao Q W, Li H, Ruan X Z, Li Y, Du J, Wu J, He L, Liu B, Zhang R and Xu Y B 2023 *Chin. Phys. Lett.* **40** 087302
[48] Park J, Rowlands G E, Lee O J, *et al.* 2014 *Appl. Phys. Lett.* **105** 102404